**Magnesium Technology 2013**
*Edited by: Norbert Hort, Suveen N. Mathaudhu, Neale R. Neelameggham, and Martyn Alderman*
***TMS (The Minerals, Metals & Materials Society), 2013***

# NUCLEATION KINETICS OF THE γ-PHASE IN A BINARY MG-AL ALLOY

Mehdi Lalpoor[1,2], J.S. Dzwonczyk[1,2], N. Hort[3], S.E. Offerman[2]
[1]Materials innovation institute, Mekelweg 2, 2628 CD Delft, The Netherlands
[2]Delft University of Technology, Department of Materials Science and Engineering, Mekelweg 2, 2628 CD Delft, The Netherlands
[3]Magnesium Innovation Center, Helmholtz Zentrum Geesthacht, Max-Planck-Straße 1
21502 Geesthacht, Germany

Keywords: Mg-Al alloys, precipitation, Nucleation kinetics

## Abstract

The binary magnesium-aluminum system has been studied extensively the last decades. Surprisingly, the kinetics of nucleation of the γ-precipitates ($Mg_{17}Al_{12}$) in the α-matrix have not been determined experimentally in detail. The main goal of this research is to investigate the precipitation kinetics of the γ-phase in a Mg-Al alloy during annealing, and to understand the relation between the precipitate volume fraction and the mechanical properties of the material. Comprehensive micro-structural analysis was undertaken to reveal the number density, volume fraction, and morphological changes of the γ-precipitates after solution heat treatment (homogenization) and during subsequent annealing below the solvus temperature. As a result, the incubation time and steady state nucleation rate of γ-precipitates in the α-matrix were determined by fitting the experimental data to the classical nucleation theory.

## Introduction

The burst in the global population in the next few decades has made new concerns regarding the materials consumption and environmental issues[1]. Replacement of regular alloys such as aluminum and steel in transportation means by lighter ones such as magnesium helps reduce the fuel consumption and $CO_2$ emission. Magnesium is a light metal which is readily available and has excellent castability [2], but its low yield strength, yield strength anisotropy and poor room temperature formability [3-5]have resulted in the development of Mg-alloys chiefly as cast products. The high strength of cast products obtained by solid solution and precipitation hardening is mainly due to the addition of rare earth metals (RE's) [6]. The similar electrochemical potential of RE's to Mg helps improve the corrosion resistance, and the high melting point precipitates formed by them increase the creep resistance, strength and ductility of Mg-alloys [7].However, the rare earth alloying elements that provide magnesium alloys with high strength, high ductility, creep and corrosion resistance should be avoided in the near future due to their high price and risk of supply disruption[8]. Therefore, in order to gain high strength and high ductility in Mg-alloys in the absence of RE elements other strengthening mechanisms must be applied while using abundantly available elements. Severe plastic deformation may be used to modify the texture by rearrangement of the distribution of basal planes [9] in order to improve the ductility, since the critical resolved shear stress (CRSS) for basal plane slip in Mg is ~100 times lower than that for non-basal plane slip. The grain size reduction is also an efficient strengthening mechanism in Mg alloys because the Hall-Petch coefficient for magnesium is reported to be approximately 0.7 MP $m^{-1/2}$ for coarse grains (30-87 μm) and 0.13 MPa $m^{-1/2}$ for fine grains (17-30 μm) [10], which is significantly higher compared to aluminum alloys (0.07 MPa $m^{-1/2}$) [11, 12]. Precipitation hardening, which is widely practiced in aluminum alloys, would be another potential strengthening mechanism, however, not so efficient for magnesium alloys due to their low precipitation hardening response. It has been long known that age-hardening response of Mg alloys is poor compared with many age-hardenable aluminum alloys.

Among the abundantly available elements, Al has the highest solubility in Mg at elevated temperatures (12.6 wt.% at 437 °C), which falls to about 2% at room temperature [13]. In spite of this, Al fails to act as an efficient precipitation hardenable element in Mg. The main reason for the poor age-hardening response of Mg-Al based alloys has been attributed to the coarseness and unfavorable orientation of the continuous precipitates with respect to the basal plane of Mg, which makes them inefficient obstacles to dislocation movement [14-16]. The age hardening response of magnesium alloys may be enhanced by promoting precipitates on the most effective planes for strengthening. However, the promotion of prismatic or pyramidal precipitates in magnesium alloys is difficult since the factors that contribute to the choice of precipitates morphology are not fully understood [17]. The number density of precipitates may be enhanced by increasing the number of potential nucleation sites, which would result in increased precipitation hardening. While such technical solutions are practically applied to stimulate the aging response of Mg-Al alloys, a thorough understanding of the nucleation mechanism sounds essential. The overall kinetics of precipitation of some Mg-Al alloys have been investigated [18, 19], however the nucleation kinetics of such alloys are not studied yet. In this research work the nucleation kinetics of a Mg-7 wt.% Al alloy are studied with the aim to understand the slow precipitation response of such alloys during heat treatment. Using the classical nucleation theory, the incubation time and steady state nucleation rate are assessed for the first time.

## Experimental procedure

The material used in this project was a Mg-7 wt.% Al alloy produced by permanent mold casting in the form of a 100 mm diameter cylinder. The as-cast microstructure consisted of coarse γ-$Mg_{17}Al_{12}$ constituents in an α-Mg matrix. After cutting, a big piece of alloy was encapsulated in a quartz tube filled with argon and sealed in order to prevent oxidation at elevated temperatures. The solution heat treatment was performed at 425 °C for 160 hours and the XRF as well as EPMA experiments proved that Al is homogenously distributed in the matrix. After the end of solution heat treatment the tube was broken and the sample was quenched in water. The precipitation hardening was performed at 260 °C for various times namely, 10 and 30 min, 1, 2, 3, 5, 10, 12, 15 and 24 h. The samples were enclosed in steel envelopes flushed with argon for protection against oxidation and they were

immediately quenched in water afterwards. In order to reveal the microstructure and quantify the number density as well as volume fraction of the precipitates, the samples were mechanically ground/polished and then etched in 1% Nital solution for 1 minute. Due to the importance of statistical reliability of data, the scanning electron microscopy (SEM) was used to be able to cover a large area including multiple grains. Image analysis was performed on the back scattered electron images to determine the number density and volume fraction of the precipitates. The areas covered per image were 16×21 $\mu m^2$ for samples annealed for short times, 61×81 $\mu m^2$ for 5 h to 12 h annealing, and 93×123 $\mu m^2$ for samples annealed longer than 12 h. 30 images were analyzed to determine the number density and 20 images for volume fraction of the precipitates, and the average values are reported here.
The micro-hardness tests were performed using the Struers-Dura Scan 70 machine with an indentation load of 100 g. 40 indentations were done for each case in grids of 4×10 points 200 μm away from each other, and the average values were calculated. Thus, an area of 1.1 $mm^2$ was covered in order to assure the statistical reliability of the data.

**Results and discussion**

Fig. 1 shows the evolution of microstructure in the Mg-7 wt% Al alloy after various heat treatment conditions. As can be seen in Fig. 1a, some precipitates have formed right after quenching of the solution heat-treated sample. Our observations indicated that there is no noticeable change in the number as well as volume fraction of the γ-precipitates during the early stages of precipitation hardening treatment, i.e. from t = 0 min to t = 3 h. It is only after 5 hours annealing that the precipitates start showing up on the microstructure (Fig. 1b). From this moment on, the volume fraction and number density of the precipitates increase drastically up to 12 h annealing (Fig. 1c). After 12 h annealing however, the number density of the precipitates start to fall sharply due to coarsening while the volume fraction remains constant (Fig. 1d). The precipitates have a lath shape and grow both in thickness and length with increasing annealing time as observed from the SEM images.
Fig. 2a shows the changes in the volume fraction of γ-precipitates with aging time at 260 °C. As explained before, the volume fraction of the precipitates starts increasing only after 5 h (18,000 s) annealing and gains its equilibrium value predicted by the phase diagram (4.96%) after 12 h (43,200 s). By applying the lever rule (Eq. 1) to the volume fractions measured through image analysis, the aluminum weight fraction of the matrix as a function of annealing time was calculated [20] (Fig. 2b).

$$X_{Al}^{\alpha-Mg}(t) = \frac{X_0 - f^{\gamma}(t) \cdot {}^{e}X_{Al}^{\gamma}}{1 - f^{\gamma}(t)} \qquad (1)$$

Where, the $f^{\gamma}(t)$ is the volume fraction of the precipitates, $X_0 = 0.07$ and ${}^{e}X_{Al}^{\gamma} = 0.44$. The driving force for nucleation was calculated by Thermo-Calc for various aluminum concentrations of the matrix starting from a supersaturated solid solution up to the end of transformation where the equilibrium aluminum concentration corresponding to 260 °C is reached (~ 4.68 wt.%). Knowing the changes in aluminum concentration of the matrix with time (Fig. 2b), the time dependence of the driving force for nucleation was determined correspondingly and the results are presented in Fig. 2c. As can be seen, the driving force is initially high (where the aluminum concentration of matrix is high) and it decreases as the precipitation proceeds.

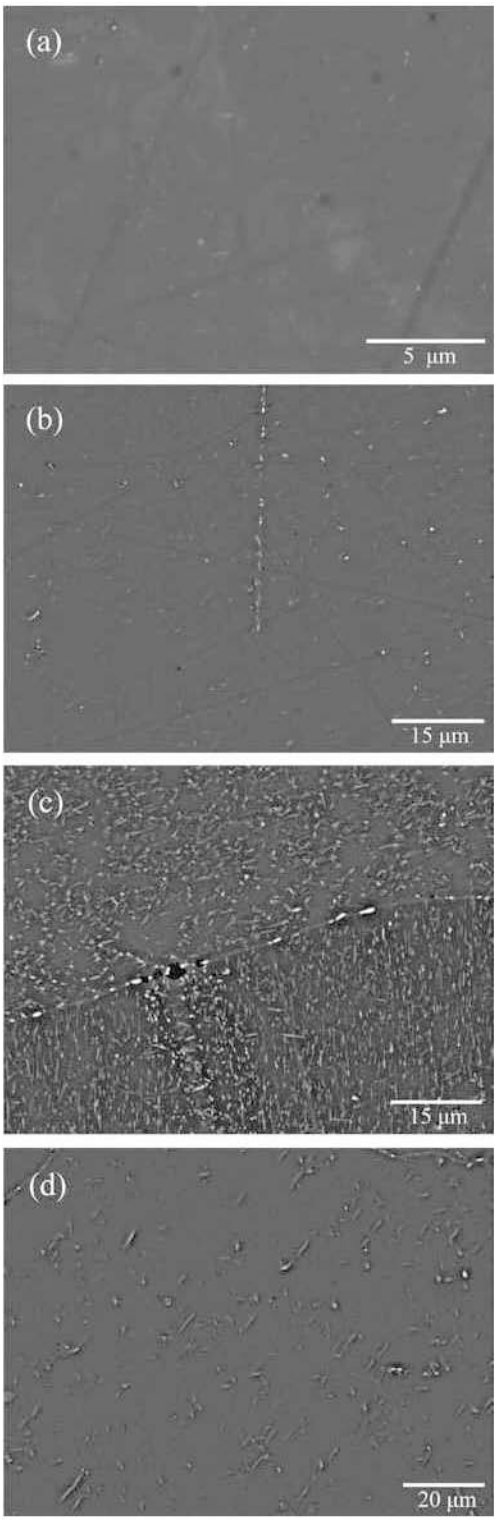


Figure 1. Evolution of microstructure of the Mg-7 wt.% Al alloy under various heat treatment conditions: a) solution heat treated at 425 °C and quenched, b, c and d) precipitation hardened at 260 °C for 5, 12 and 15 hours respectively (mind the different magnifications).

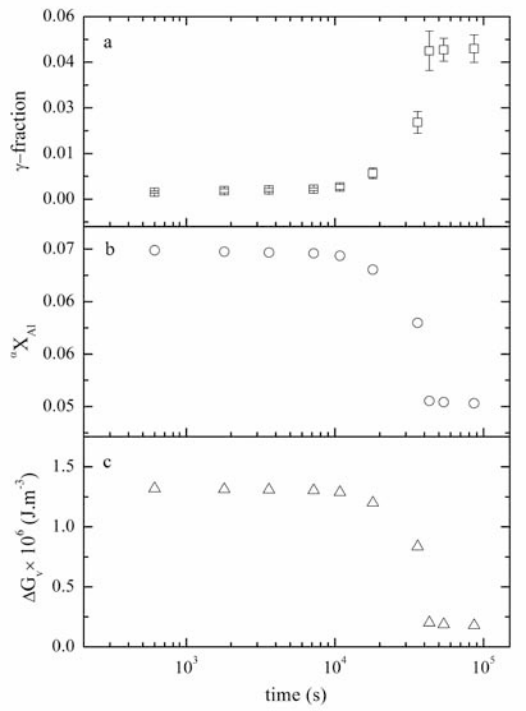


Figure 2. The results of quantitative metallography and thermodynamic calculations: a) volume fraction of the γ-precipitates ($Mg_{17}Al_{12}$) measured from SEM images, b) the aluminum weight fraction of the α-Mg matrix versus annealing time calculated using Eq. 1, and c) the driving force for nucleation; $\Delta G_v$, versus annealing time (calculated by Thermo-Calc).

Fig. 3a shows the number density of precipitates measured form the SEM images. The number density remains very low up to 5 h (18,000 s) and then increases sharply until 12h (43,200 s) annealing after which it drastically falls due to the coarsening of the precipitates. The number densities of the precipitates in this alloy are an order of magnitude smaller compared to the ones reported for AZ91 at 250 °C [14]. The higher concentration of the precipitates in AZ91 may be on the one hand attributed to the higher Al content of the matrix which enhances the chemical driving force of nucleation. The addition of Zn on the other hand, reduces the solid solubility of aluminum in magnesium and increases the amount of precipitate phase formed upon aging [14]. In Fig. 3b, the nucleation rate has been calculated per untransformed fraction of the matrix ($1-f^{\gamma}$). The large errors at small annealing times are due to the small time steps and tend to decrease with increasing the aging time. As can be seen, the nucleation passes through a relatively long incubation period after which the rate increases dramatically up to 12 h (43,200 s). Afterwards, due to very rapid coarsening the nucleation rate turns to negative, which is not presented in the graph. In order to quantify the nucleation kinetics, the classical nucleation theory was applied, as our observations indicated that the nucleation mechanism is homogenous and occurs predominantly within the grains.

Having fitted the classical nucleation theory (Eq. 2) to the experimental results gained in this study, it turned out that the results barely fit to the initial increasing exponential part of the curve ($\exp\left(-\frac{\tau}{t}\right)$), and the other part which comprises the decrease of the nucleation rate due to driving force reduction ($\exp\left(-\frac{\psi/\left(\Delta G^{*}\right)^{2}+Q_d}{kT}\right)$) does not appear owing to the immediate coarsening that follows the nucleation rate peak.

$$\dot{N}_u = \dot{N}_{u,ss}\exp\left(-\frac{\tau}{t}\right) = N\cdot\beta^{*}\cdot Z\cdot\exp\left(-\frac{\psi/\left(\Delta G^{*}\right)^{2}+Q_d}{kT}\right)\cdot\exp\left(-\frac{\tau}{t}\right) \qquad (2)$$

In Eq. 2, $N$ is the density of the potential nucleation sites, $\beta^{*}$ is the frequency factor, or rate at which single solute atoms are added to the critical nucleus, $Z$ is the Zeldovichnon-equilibrium factor, ψ contains information on the interfacial energy, $\Delta G^{*}$ is the free energy of activation for the formation of the critical nucleus, $Q_d$ the activation energy for diffusion of Mg in Al, $k$ Boltzmann constant, $T$ absolute temperature, $\tau$ incubation time, and $t$ the annealing time.

The fact that the entire classical nucleation equation could not be fitted to the experimental results (shown in Fig. 2b) inhibited us from direct assessment of ψ, and surface energy of the precipitates accordingly. However, by fitting the $\dot{N}_u = \dot{N}_{u,ss}\exp\left(-\tau/t\right)$ curve to the experimental data (Fig. 3b), one gets the steady state nucleation rate $\dot{N}_{u,ss}$=1.6×10$^{14}$ ± 2.7×10$^{13}$ m$^{-3}$s$^{-1}$ and the incubation time$\tau$ = 74210.1 ± 6438.1 s as the fitting parameters. Selecting lower aging temperatures may help prevent rapid coarsening, but the longer incubation periods expected at such low temperatures makes the aging time required to reach the steady state nucleation rather long [14].

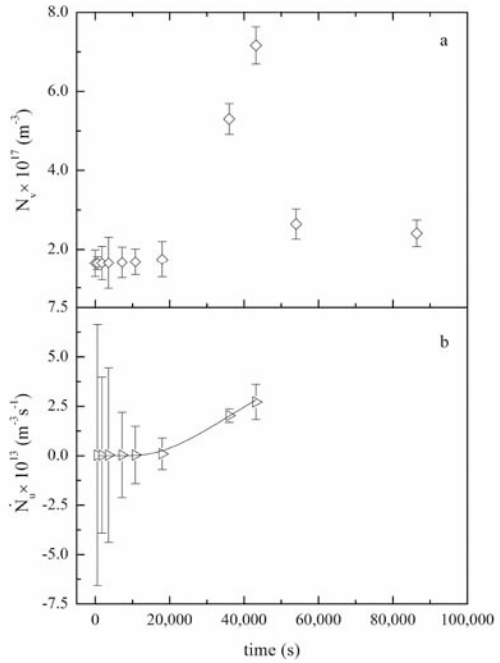


Figure 3. Evolution of precipitates number density and nucleation rate in the course of precipitation hardening: a) the number of precipitates per unit volume plotted versus annealing time in the Mg-7 wt.% Al alloy, b) the nucleation rate up to 12 hours annealing (due to rapid coarsening after 12 h, the nucleation rate is not plotted). The solid line is a fit of $\dot{N}_u = \dot{N}_{u,ss}\exp\left(-\tau/t\right)$.

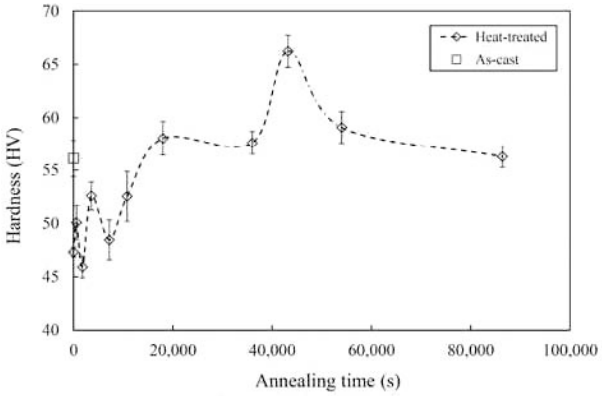


Figure 4. The results of micro-hardness tests on Mg-7 wt.% Al alloy in as-cast and after various heat treatment conditions.

The age hardening response of the Mg-7 wt.% Al can be seen from Fig. 4. The hardness of the alloy in the as-cast condition is 56.1 ± 1.7 HV, but after solution heat treatment and quenching it falls to 47.3 ± 0.5 HV. The hardness values fluctuate from t = 0 up to 3 h (10,800 s) annealing and then reach a plateau at 5 h (18,000 s). The hardness peak (66.2 ± 1.5 HV) is reached after 12 h (43,200 s), which is in agreement with our number density and volume fraction measurements. After 12 h annealing when coarsening becomes dominant, the hardness falls and eventually reaches 56.3 ± 1.0 HV at t = 24 h (86,400 s). The peak hardness value is only 18% higher than the as-cast condition and 40% higher than the solution heat treated state indicating that under normal conditions the aging response of the material is rather low. Another interesting observation in this study was the stimulated nucleation of precipitates on the deformation bands formed during the sample preparation prior to aging treatment (Fig. 5; the precipitates formed on deformation bands are not included in the number density and volume fraction measurements). In the corresponding sample (aged at 260 °C for 5 h), while the number density of the precipitate is slightly higher compared to the sample aged for 3 h, the deformation bands have acted as potential nucleation sites and apparently reduced the energy barrier for the nucleation. This observation strengthens the idea that the plastic deformation prior to aging may be used as an effective tool for improvement of the aging response in magnesium alloys.

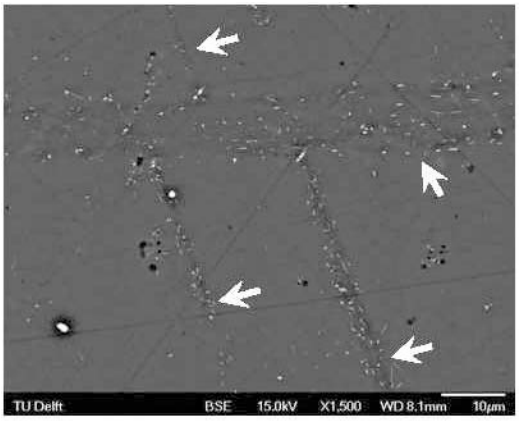


Figure 5. Microstructure of the Mg-7 wt.% Al alloy after 5 h annealing at 260 °C. The role of deformation bands in stimulating the nucleation is indicated by arrows.

## Conclusions

The nucleation of the $Mg_{17}Al_{12}$ precipitates in the Mg-7 wt% Al alloy remains in the transient state and coarsening occurs before reaching the steady state regime, which makes the direct assessment of the precipitate's interfacial energy from the entire nucleation curve impossible. While the nucleation rate is rather low during the incubation period, any external parameter may stimulate the nucleation. The deformation bands accidentally formed during cutting of the samples before annealing acted as efficient nucleation sites. This observation is a proof that deformation prior to precipitation hardening may help improve the aging response of Mg-alloys.

## Acknowledgments

This research was carried out under the project number M42.5.10395 in the framework of the Research Program of the Materials innovation institute M2i (www.m2i.nl).

## References

[1] R. Dobbs, J. Oppenheim, F. Thompson, M. Brinkman, M. Zornes, in, McKinsey Global Institute, 2011.
[2] K. Hono, C.L. Mendis, T.T. Sasaki, K. Oh-ishi, Scripta Materialia 63 (2010) 710–715.
[3] I.J. Polmear, Light Alloys; From Traditional Alloys to Nanocrystals, Elsevier Butterworth-Heinemann, Oxford, 2006.
[4] J. Koike, T. Kobayashi, T. Mukai, H. Watanabe, M. Suzuki, K. Maruyama, K. Higashi, Acta Materialia, 51 (2003) 2055–2065.
[5] J. Bohlen, P. Dobron, E.M. Garcia, F. Chmelik, P. Lukac, D. Letzig, K.U. Kainer, Advanced Engineering Materials, 8 (2006) 422-427.
[6] I.J. Polmear, Materials Science and Technology January 1994 Vol. 10 1, 10 (1994 ) 1-16.
[7] S.K. Das, L.A. Davis, Materials Science and Engineering, 98 (1988) 1-12.
[8] S.W. Xu, K. Oh-ishi, S. Kamado, F. Uchida, T. Homma, K. Hono, Scripta Materialia 65 (2011) 269–272.
[9] W.J. Kim, H.G. Jeong, H.T. Jeong, Scripta Materialia 61 (2009) 1040–1043.
[10] J. Koike, Metallurgical and Materials Transactions A, 36 (2005) 1689-1696.
[11] T. Mukai, K. Higashi, Scripta Materialia, 44 (2001) 1493–1496.
[12] J.W. Wyrzykowski, M.W. Grabski, Philosophical Magazine A, 53 (1986) 505-520.
[13] H. Okamoto, Desk handbook phase diagrams for binary alloys, ASM International, Materials Park, OH 44073-0002, 2000.
[14] S. Celotto, Acta Materialia, 48 (2000) 1775-1787.
[15] A.F. Crawley, B. Lagowski, Metallurgical Transactions 5(1974) 949-951.
[16] A.F. Crawley, K.S. Milliken, Acta Metallurgica, 22 (1974) 557-562.
[17] C.L. Mendis, K. Oh-ishi, Y. Kawamura, T. Honma, S. Kamado, K. Hono, Acta Materialia, 57 (2009) 749–760.
[18] D. Duly, Y. Brechet, B. Chenal, Acta Metall. Mater. , 40 (1992) 2289-2300.
[19] B.A. Esgandari, H. Mehrjoo, B. Nami, S.M. Miresmaeili, Materials Science and Engineering A 528 (2011) 5018–5024.
[20] S.E. Offerman, H. Strandlund, N.H.v. Dijk, J. Sietsma, E.M. Lauridsen, L. Margulies, H.F. Poulsen, J. Ågren, S.v.d. Zwaag, Materials Science Forum 550 (2007) 357-362.